Space Variance Analysis of the SAR Acquisition Geometry for ROSE-L Images

Valeria Gracheva[a], Pau Prats-Iraola[b], and Marc Rodriguez-Cassola[b]
[a]European Space Agency (ESA), Keplerlaan 1, 2201 AZ, Noordwijk, The Netherlands
[b]DLR Microwaves and Radar Institute, Muenchener Str. 20, 82234 Oberpfaffenhofen, Germany

Abstract

In this paper the efficient kernel evaluation technique is extended and used to analyze the impact of space variance of the SAR acquisition geometry on ROSE-L SAR images, in particular when Fourier-based focusing kernels are used. The idea of the efficient kernel evaluation technique is to perform a numerical calculation of the focusing performance for a given mission with the corresponding orbit and system parameters. This assessment can be performed for several geographical locations in order to obtain the global performance of the focusing kernel. Based on the obtained results and considering the system requirements, it shall be decided whether the space variance needs to be accommodated with additional processing steps. The use of such a tool allows for the design of the focusing kernel prior to the actual implementation and validation with time-domain simulations of point targets.

1 Introduction

Future spaceborne synthetic aperture radar (SAR) systems are being developed to deliver high spatial resolution products with stringent requirements on the ground processor performance in terms of the impulse response function (IRF) parameters, like for example the geolocation error or deviations between nominal and measured resolution. However, azimuth variance and topography can impact the performance of the focusing kernel significantly. Azimuth variance referes to azimuth dependence of the effective velocity along the azimuth dimension for targets located at the same range distance and the same topographic height. A given image is focussed with the range history from the middle of the burst. Due to the azimuth variance of the geometry from the curved orbit and the Earth's rotation, the range history however varies in azimuth. Therefore, the matched filter is tuned for the middle of the processing block might result in a degraded IRF as we move away from the middle. The mismatch due to topography refers to the assumption of the focusing kernel that the height of the target is equal to a given reference height. If this is not true then the range history of the target is a different one as assumed by the kernel, which leads to IRF degradation similar as the azimuth variance. The impact of azimuth variance and topography depends on the system parameters of the SAR system (azimuth resolution, imaging mode, image size,...), the orbit and the latitude of the scene. One possibility to analyze if azimuth variance and topography will impact the products of a future SAR system significantly is by simulating raw data with point targets at the edges of the image, developing a focusing kernel for the SAR system under consideration, processing the simulated data with this focusing kernel and then analyzing the impulse response function (IRF) parameters of these point targets. The simulation and processing has then to be repeated for a large set of latitudes, because the impact of azimuth variance and topography are latitude dependent. The drawback of this method is that it is computationally expensive and that for new missions also a focusing kernel has to be developed.

This paper uses a different approach as a first assessment before going into the actual implementation of the processor. Here the methodology proposed in [1] is used. The idea of this methodology is to quantify the performance of a focusing kernel without having to implement the processor itself nor perform a costly point-target simulation. The methodology is based on the computation of the transfer function of the focusing kernel, and hence convenient for Fourier-based processing algorithms. This transfer function is compared to the frequency responses of the point targets, which are computed numerically using their range histories. The difference can be directly evaluated to assess the performance of the focusing kernel. The methodology is valid as long as a large time-bandwidth product applies, which is the usual case in current air- and spaceborne SAR systems.

The contribution of this paper is the extension of the existing efficient evaluation tool to consider all geographical locations, the topography impact and also to operate for a ScanSAR system. Furthermore, in this paper the current ROSE-L orbit and system parameters are used to evaluate the impact of azimuth variance and topograpy on the quality of future ROSE-L products. ROSE-L (Radar Observation System for Europe at L-band) is supposed to launch in 2028 and it will carry an L-band SAR system as part of the Copernicus Expansion Programme [2].

This paper is organized as follows: In Section 2 the general methodology of the SAR Focusing Kernel Efficient Evaluation is described and it outlines how this evaluation is

Table 1 Orbit Parameters

Repeat cycle	12 days
Semi-major axis	7070978.894 m
Eccentricity	0.001181°
Inclination	98.120°
Right Ascension	250270.149°
Argument of Perigee	90.008°
Mean Anomaly	270.149°
Satellite velocity	7600 m/s
Look Direction	Right
Pass	Ascending

Table 2 System Parameters

Center frequency	1.2575 GHz
Swath width	88 km
Incidence Angle	28.235°
Burst duration	1.104 s
Range Bandwidth	65.25 MHz
Pulse Length	48.08 μ s
ScanSAR Doppler Bandwidth	629.47 Hz
Full Doppler Bandwidth	2365 Hz
Slant range resolution	2 m
Azimuth resolution	10 m

used to analyse the SAR focusing kernel performance for the ROSE-L mission. The results of this analysis are shown in Section and Section concludes his paper.

2 SAR Focusing Kernel Efficient Evaluation Methodology

In Figure 1 the flow chart of the SAR Focusing Kernel Efficient Evaluation Methodology is shown. To calculate the reference longitudes and latitudes, the orbit, which was chosen for the ROSE-L mission, was computed. The parameters of this orbit are summarized in Table 1. First, an orbit with a coarse sampling was computed. Then, with the knowledge of the incidence angle, for each orbit position the corresponding longitude and latitude on the Earth's surface was calculated. For this analysis only one subswath was considered. Figure 2 shows the calculated reference longitudes and latitudes, which are used as an input to the efficient kernel evaluation tool. For each of these Earth's surface points the focusing performance is analyzed.

One reference latitude and longitude is considered as the center position of one acquired scene. The orbit around the center position is interpolated, so that the sampling corresponds to 1/PRF. With this orbit the target's range history is computed, which is equal to

$$R(t_a) = ||\mathbf{x}_t - \mathbf{x}_s(t_a)||, \tag{1}$$

where $\mathbf{x}_t$ are the target's coordinates and $\mathbf{x}_s(t_a)$ are the satellite coordinates at a given azimuth time t_a.

The efficient kernel evaluation tool needs the system parameters of the considered SAR mission as an input. The system parameters of ROSE-L, which were used in this paper are summarized in Table 2.

The target's and kernel's phase were derived in [1] and also validated with time-domain simulations followed by true processing. Note that this equation (and the following) assumes two-way range histories. Here only the key steps are summarized.

To calculate the target's phase in the 2D-frquency domain, the first step is to start at the spectrum of a range-compressed point target in the range frequency-azimuth time domain, which is well known as [3]

$$H(f_r, t_a) = \exp\left[-\mathrm{j}\cdot\frac{2\pi}{\mathrm{c}}\cdot(f_0+f_r)\cdot R(t_a)\right] \tag{2}$$

if the amplitude terms can be neglected. Here c is the speed of light, f_0 is the central frequency, f_r is the range frequency and t_a is the azimuth time.

To perform the azimuth FT, the principle of stationary phase has to be applied. This requires the computation of the stationary time t_a^*, being the one satisfying [3]

$$\left.\frac{\partial R(t_a)}{\partial t_a}\right|_{t_a=t_a^*} = -\frac{\mathrm{c}\cdot f_a}{f_0+f_r}, \tag{3}$$

where f_a is the azimuth frequency. After evaluating (3) for each point of the 2D spectrum, the phase of the FT of (2) can be approximated by

$$\varphi_T(f_r, f_a) \approx -\frac{2\pi}{\mathrm{c}}\cdot(f_0+f_r)\cdot R(t_a^*) - 2\pi\cdot f_a\cdot t_a^*, \tag{4}$$

To solve for t_a^*, series reversion is used by by first expressing $R(t_a)$ as a power series of t_a [4].

The kernel's phase can of the different focusing kernels can be found in the literature. Here the range-Doppler kernel was used, which transfer function can be found in [3] as

$$\begin{aligned}\varphi_{RD}(f_r,f_a) \quad = \quad & -\tfrac{4\pi}{\lambda}\cdot r_{ref}\cdot\sqrt{\left(1+\tfrac{f_r}{f_0}\right)^2-\left(\tfrac{\lambda\cdot f_a}{2\cdot v_{e,ref}}\right)^2} \\ & + 2\pi\cdot\Delta t_{r,RD}(f_a)\cdot f_r \\ & - \tfrac{4\pi}{\lambda}\cdot[r_0\cdot\gamma(f_a,v_e) - r_{ref}\cdot\gamma(f_a,v_{e,ref})],\end{aligned} \tag{5}$$

where r_{ref} is the closest approach distance, v_e is the effective velocity, r_{ref} is the closest approach distance for the reference target, $v_{e,ref}$ is the effective velocity of the reference range, and the residual RCM is given by

$$\Delta t_{r,RD}(f_a) = -\frac{2}{\mathrm{c}}\cdot\left(\frac{r_0}{\gamma(f_a,v_e)} - \frac{r_{ref}}{\gamma(f_a,v_{e,ref})}\right) \tag{6}$$

and

$$\gamma(f_a, v_e) = \sqrt{1-\left(\frac{\lambda\cdot f_a}{2\cdot v_e}\right)^2}. \tag{7}$$

The first term in (5) is the matched filter performed in the 2D frequency domain at the beginning of the processing

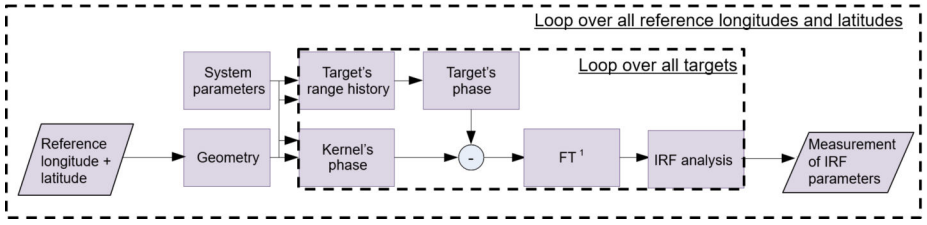

Figure 1 Flow chart of the efficient evaluation procedure

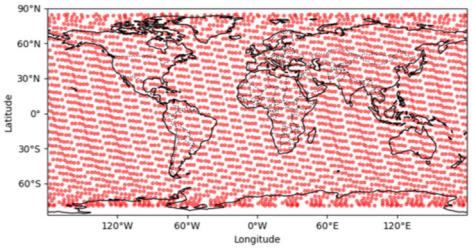

Figure 2 Reference latitudes and longitudes, which were used in this analysis.

tuned at r_{ref}, the second term performs the residual range cell migration, while the last one performs the residual azimuth compression.
As shown in Figure 1 the next step is to subtract the kernel's phase from the target's phase. Ideally, both phases should be equal and therefore the result should be zero. The resulting impulse response function (IRF) in the time domain is

$$h(t_r, t_a) = \mathrm{FT}_{2D}^{-1}\{\, \{W(f_r, f_a) \cdot \exp\left[\mathrm{j} \cdot \varphi_{error}(f_r, f_a)\right]\} \,\}, \tag{8}$$

where $\varphi_{error}(f_r, f_a) = \varphi_T(f_r, f_a) - \varphi_K(f_r, f_a)$ and t_r refers to fast time. $W(f_r, f_a)$ considers the windowing in the 2D frequency domain. Here only a rect-window was applied to filter to the corresponding range and azimuth frequency of the system. But of course also different windows like the Hamming window could also be applied. $h(t_r, t_a)$ can then be treated like the IRF of a simulated point target or a corner reflector of real data after focusing. Therefore the same module was used to perform the IRF analysis of $h(t_r, t_a)$, as is also used for the end-to-end simulators and prototype processors.
For the ROSE-L mission the ScanSAR imaging mode will be used. To consider this mode, the efficient kernel evaluation tool needed further adjustments. The scene size was calculated according to the burst length defined in Table 2. Furthermore, for the windowing in the 2D frequency domain $W(f_r, f_a)$ the Doppler centroid of each target was calculated and the windowing was then performed around this Doppler centroid and by considering the ScanSAR azimuth bandwidth, not the full azimuth bandwidth.
The highest impact of azimuth variance is visible at the edges of the burst. Therefore, to evaluate this impact, three IRFs were calculated. One at the beginning (in azimuth), one at the middle and one at the end of the burst. All IRFs were calculated for the center slant range. The results of the evaluation of these IRFs with the efficient kernel evaluation tool are shown in Section 3.1.
To analyze the topography dependence, again three IRFs were calculated. The position of all three IRFs are equal in the radar coordinates, namely at the beginning of the burst and for the center slant range. But the heights of these targets were chosen differently. The height of the first target is equal to 0 m, the height of the second one is equal to 750 m and the one of the third target is equal to 1500 m. The results of this evaluation is shown in 3.2.
The evaluation in Section 3 focuses just on the focusing kernel. Therefore, antena pattern or other instrument effects are not being considered.

3 Results

In this section the results of the efficient kernel evaluation for different target positions are shown. As described by Figure 1, for each reference latitude and longitude, which are shown in Figure 2, the IRF for different target positions is calculated by using the approach described in Section 2. Then for each target the IRF analysis module is used to measure the IRF parameters, namely the resolution, position error, peak-to-sidelobe ratio (PSLR) and integrated sidelobe ratio (ISLR). These values are then stored for each reference latitude and longitude and then interpolated and plotted on a map, as shown in Sections 3.1 and 3.2. In these sections only the azimuth IRF paramters are shown, because the range IRF parameters are hardly affected by azimuth variance and topography for the ROSE-L scenario.

3.1 Azimuth Variance Results

Figure 3 shows the azimuth error in percent on a map for the three different target positions. The same arrangement is used in Figure 4 to show the position error in azimuth of the three target positions and Figures 5 and 6 show the peak-to-sidelobe ratio (PSLR) and integrated sidelobe ratio (ISLR) of the three target positions. Figure 3 shows that an azimuth resolution error does not occur for any of the three targets. In Figure 4, however, a position error of more than 20 cm is evident for the targets at the beginning and the end of the burst. The maximum position error occurs around approximately the latitude of 40°N. The position error occurs as a consequence of the matched filter mis-match at the edges of the burst due to azimuth variance. For a stripmap imaging mode this mis-match would result in a worsening of the azimuth resolution. But for ScanSAR, due to the bandpass filtering around the Doppler

centroid, the described mis-match produces undesired azimuth shifts. This distortion was also described in [5] for the TOPS imaging mode. There are no position errors in azimuth for the target at the center of the burst, because here the azimuth matched filter assumes the correct range history. Figures 5 and 6 show that the PSLR and ISLR are unaffected by the filter mis-match at the edges of the burst.

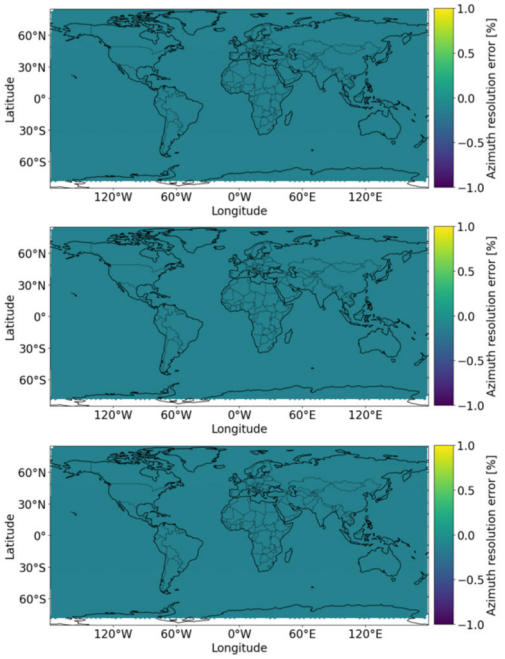

Figure 3 Azimuth resolution error in percent in dependence of latitude and longitude for target at beginning of the burst (top), middle of the burst (middle), end of the burst (bottom).

3.2 Topography Dependence Results

Figures 7 - 10 show the azimuth IRF parameters of a target at 750 m height (on the top) and for a target at 1500 m height at the beginning of the burst in azimuth. The IRF parameters of the reference target at 0 m are found in Section 3.1 at the top of each figure. The impact of the topography dependence is similar as the one of azimuth variance. Because of the range history dependency on the target's height, a mis-match of the azimuth filter results for target heights different than zero. Also for the topography dependence, due to the ScanSAR imaging mode, undesired azimuth shifts are the result of this mis-match and not an azimuth resolution loss. Figure 8 shows that for target's heights of 1500 m position errors of around 2 m have to be considered. Figures 7, 9 and 10 show that other azimuth IRF parameters are hardly affected by the taget's height.

4 Conclusion

In this paper the efficient kernel evaluation method was extended to analyze the IRF parameters for different geographical locations and to also consider the ScanSAR imaging mode. Furthermore this tool was used to evaluate possible IRF parameter degradations due the azimuth

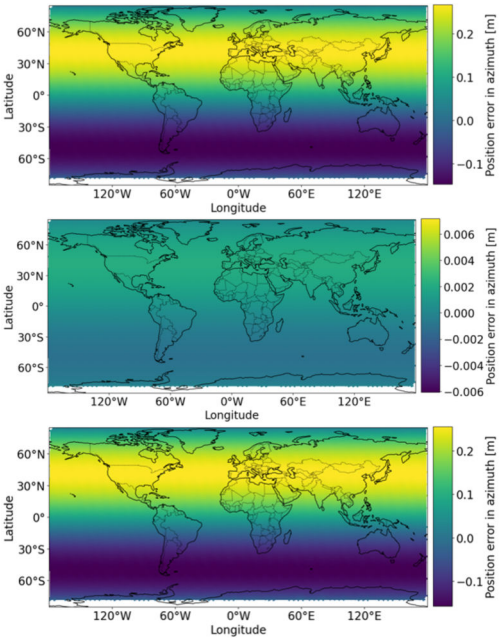

Figure 4 Position error in azimuth in dependence of latitude and longitude for target at beginning of the burst (top), middle of the burst (middle), end of the burst (bottom).

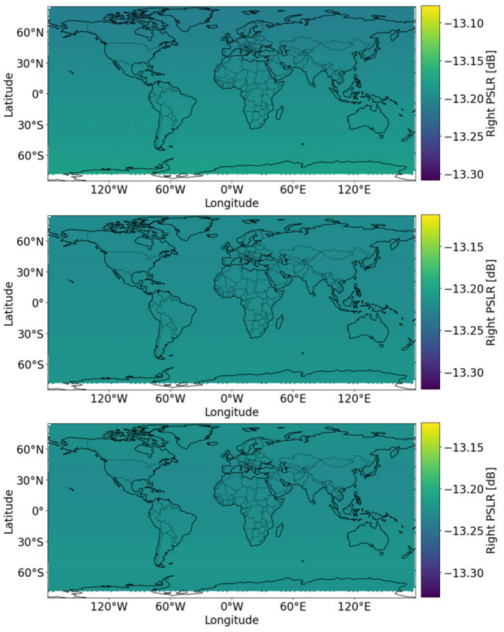

Figure 5 PSLR in dependence of latitude and longitude for target at beginning of the burst (top), middle of the burst (middle), end of the burst (bottom).

variance and topography for the ROSE-L mission. This evaluation demonstrated that for the orbit and system parameters of the ROSE-L mission azimuth position errors of more than 20 cm have to be expected. Furthermore it was shown that the geolocation errors in azimuth increase significantly for the ROSE-L mission if the target's height does not match the reference one. In order to accommodate the space variance of the geometry, like the PASTA method proposed in [5] or the SATA method, which was

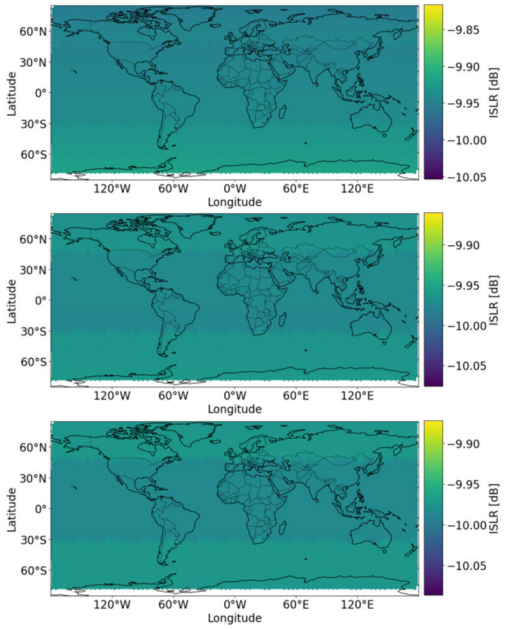

Figure 6 ISLR in dependence of latitude and longitude for target at beginning of the burst (top), middle of the burst (middle), end of the burst (bottom).

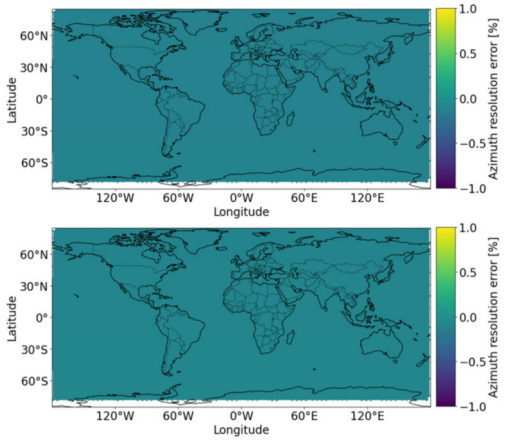

Figure 7 Azimuth resolution error in percent in dependence of latitude and longitude for target with height of 750 m (top) and with height of 1500 m (bottom).

developed in [6]. Another alternative would be to deliver annotation products with ROSE-L SAR images, which include biases, similar as the Extended Timing Annotation Dataset (EATD) of Sentinel-1 [7].

5 Literature

[1] P. Prats-Iraola, M. Rodriguez-Cassola, F. De Zan, P. Lopez-Dekker, R. Scheiber, A. Reigber, *Efficient Evaluation of Fourier-Based SAR Focusing Kernels*. IEEE Geoscience and Remote Sensing Letters, vol. 11, no. 9, pp. 1489-1493, Sept. 2014.

[2] M. Davidson, N. Gebert and L. Giulicchi, *ROSE-L – The L-band SAR Mission for Copernicus*. EUSAR 2021; 13th European Conference on Synthetic Aperture Radar, 2021, pp. 1-2.

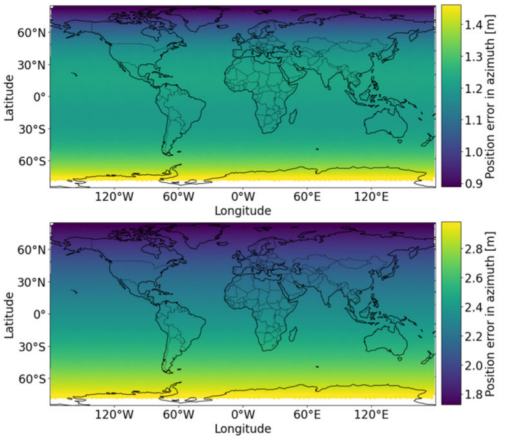

Figure 8 Position error in azimuth in dependence of latitude and longitude for target with height of 750 m (top) and with height of 1500 m (bottom).

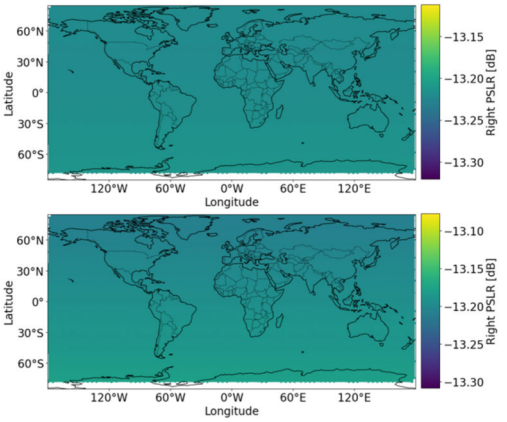

Figure 9 PSLR in dependence of latitude and longitude for target with height of 750 m (top) and with height of 1500 m (bottom).

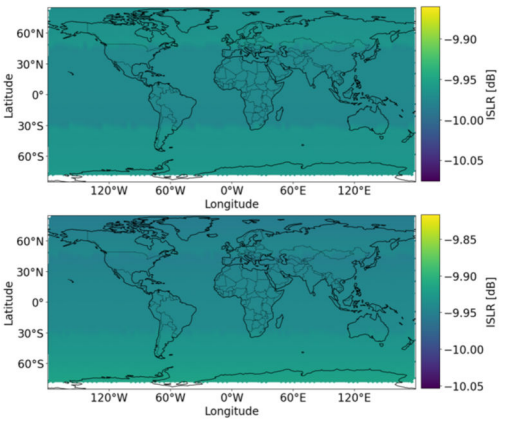

Figure 10 ISLR in dependence of latitude and longitude for target with height of 750 m (top) and with height of 1500 m (bottom).

[3] I. G. Cumming and F. H. Wong, *Digital Processing of Synthetic Aperture Radar Data. Algorithms and Implementation*. Boston, London: Artech House, 2005.

[4] Y. L. Neo, F. Wong, and I. G. Cumming, *A two-*

dimensional spectrum for bistatic SAR processing using series reversion. IEEE Geoscience Remote Sens. Lett., vol. 4, no. 1, pp. 93–96, Jan. 2007.

[5] M. Rodriguez-Cassola, P. Prats-Iraola, F. De Zan, R. Scheiber, A. Reigber, D. Geudtner, A. Moreira *Doppler-Related Distortions in TOPS SAR Images*. IEEE TGRS, vol. 53, no. 1, Jan. 2015.

[6] P. Prats, K. A. Camara de Macedo, A. Reigber, R. Scheiber and J. J. Mallorqui, *Comparison of Topography- and Aperture-Dependent Motion Compensation Algorithms for Airborne SAR*. IEEE Geoscience and Remote Sensing Letters, vol. 4, no. 3, pp. 349-353, July 2007.

[7] https://sentinels.copernicus.eu/web/sentinel/missions/sentinel-1/data-products/etad-dataset